Probing the Role of Negatively Charged Amino Acid Residues in Ion Permeation of Skeletal Muscle Ryanodine Receptor

Ying Wang,* Le Xu,* Daniel A. Pasek,* Dirk Gillespie,† and Gerhard Meissner*
*Department of Biochemistry and Biophysics, University of North Carolina, Chapel Hill, North Carolina 27599-7260; and
†Department of Molecular Biophysics and Physiology, Rush University Medical Center, Chicago, Illinois 60612

ABSTRACT Sequence comparison suggests that the ryanodine receptors (RyRs) have pore architecture similar to that of the bacterial K^+ channel KcsA. The lumenal loop linking the two most C-terminal transmembrane spanning segments in the RyRs has a predicted pore helix and an amino acid motif (GGGIG) similar to the selectivity filter (TVGYG) of KcsA identified by x-ray analysis. The RyRs have many negatively charged amino acid residues in the two regions linking the GGGIG motif and predicted pore helix with the two most C-terminal transmembrane spanning segments. We tested the role of these residues by generating single-site mutants, focusing on amino acid residues conserved among the mammalian RyRs. Replacement of two acidic residues immediately after the GGGIG motif in skeletal muscle ryanodine receptor (RyR1-D4899 and -E4900) with asparagine and glutamine profoundly affected ion permeation and selectivity. By comparison, mutagenesis of aspartate and glutamate residues in the putative linker regions showed a K^+ conductance and selectivity for Ca^{2+} compared to K^+ (P_{Ca}/P_K) close to wild-type. The results show that the negatively charged carboxyl oxygens of D4899 and E4900 side chains are major determinants of RyR ion conductance and selectivity.

INTRODUCTION

Ryanodine receptors (RyRs) are a family of Ca^{2+} release channels that play a key role in the regulation of intracellular Ca^{2+} levels by releasing Ca^{2+} from an intracellular Ca^{2+} storing compartment, the endo/sarcoplasmic reticulum (1–3). Three genes encode the mammalian RyRs, leading to the expression of three isoforms. The skeletal type RyR (RyR1) is predominantly expressed in skeletal muscle and is activated on depolarization of the cell membrane by a direct interaction with the L-type Ca^{2+} channel/dihydropyridine receptor. The cardiac type RyR (RyR2) predominates in cardiac muscle and is activated by Ca^{2+} ions that enter the cell through voltage-dependent L-type Ca^{2+} channels. The type 3 RyR (RyR3) is expressed at low levels in many cell types.

The mammalian RyRs show ~70% overall sequence identity, with the highest level of identity in the C-terminal region. In all isoforms, the C-terminal portion of the protein contains the transmembrane domain. Hydropathy analysis suggested between 4 and 12 transmembrane segments per RyR subunit (4,5). More recent studies using green fluorescent protein inserts and protease digestion indicated that each RyR1 subunit contains six to eight transmembrane helices (6). The remaining RyR amino acids form the large catalytic cytoplasmic foot structure. Cryoelectron microscopy of the RyRs reveals dimensions of 29 × 29 × 12 nm for the large cytoplasmic assembly and a 7 nm length and 8 nm diameter for the transmembrane assembly (7).

Sequence comparison suggests that the RyR ion channels have a pore architecture similar to that of some other ion channels. The lumenal loop linking the two most C-terminal transmembrane spanning segments (C-terminal loop) in the RyRs has a predicted pore helix followed by an amino acid motif (GGGIG) similar to the selectivity filter (TVGYG) identified by x-ray crystallography in a bacterial K^+ channel (KcsA; (8); see also Fig. 1). However, there exist important differences. RyRs have longer linker regions containing many negatively charged amino acid residues. They also have a relatively wide selectivity filter (≥7 Å diameter, ~10 Å long; 9–11). Moreover, the RyRs have a high ion conductance for both monovalent (~800 pS with 250 mM K^+ as conducting ion) and divalent (~150 pS with 50 mM Ca^{2+}) cations, while maintaining high divalent versus monovalent selectivity ($P_{Ca}/P_K \sim 7$ (12–14)).

A number of laboratories including our own have used mutagenesis to identify amino acid residues in the C-terminal loop of RyR1 (15) and RyR2 (16–18) that are critical for ion conductance and channel gating. Mutations of amino acid residues that are conserved in the RyRs showed significant alterations in channel activity and ion permeation as compared to wild-type-RyRs. Replacement of isoleucine in the GGGIG motif with threonine, alanine, valine, or leucine altered the sensitivity to activating Ca^{2+} and modified K^+ and Ca^{2+} ion conductances; substitution of RyR1-G4894 and the corresponding glycine in RyR2 with alanine greatly reduced the K^+ and Ca^{2+} conductances of both RyRs, while maintaining pharmacological regulation by Ca^{2+}, caffeine, and ryanodine (15,18). Replacement of the conserved negatively charged aspartate immediately after the GGGIG segment with a hydrophobic alanine or a polar, but neutral, asparagine reduced K^+ conductance, while maintaining Ca^{2+} release in a cell-based assay (15,16). Naturally occurring mutations that give rise to central core disease, a

Submitted November 9, 2004, and accepted for publication April 27, 2005.

Ying Wang and Le Xu contributed equally to this work.

Address reprint requests to Gerhard Meissner, Tel.: 1-919-966-5021; Fax: 1-919-966-2852; E-mail: meissner@med.unc.edu.

0006-3495/05/07/256/10 $2.00

doi: 10.1529/biophysj.104.056002

skeletal muscle associated disease, predominantly reside in the C-terminal loop (19).

In this study, we generated single-site mutants focusing on negatively charged amino acid residues predicted to be part of the pore region of the RyRs and conserved among the mammalian RyRs. We found that mutation of two acidic residues (D4899 and E4900) immediately after the GGGIG motif of RyR1 affected ion permeation and selectivity. By comparison, replacement of aspartate and glutamate residues with asparagine and glutamine residues in the putative linker regions bridging the two most C-terminal membrane spanning and pore helices showed a K^+ conductance and P_{Ca}/P_K close to wild-type. The results suggest that the negative charges associated with the carboxyl oxygens of D4899 and E4900 are primarily responsible for the high ion conductances and ion selectivity of RyR1. We have presented a model that supports this view (20).

EXPERIMENTAL PROCEDURES

Materials

[^{3}H]Ryanodine was obtained from PerkinElmer Life Sciences (Boston, MA), unlabeled ryanodine from Calbiochem (La Jolla, CA), Fluo-4-AM from Molecular Probes (Eugene, OR), complete protease inhibitors from Roche (Indianapolis, IN), and human embryonic kidney (HEK) 293 cells from ATCC. Phospholipids were from Avanti Polar Lipids (Alabaster, AL). All other chemicals were of analytical grade.

Construction of mutant cDNA

For construction of RyR1 mutants, the full-length rabbit RyR1 cDNA (*Cla1*/*Xba1*,*14443*/*15276*) subcloned into pBluescript vector (21) was used as template for mutagenesis. Single and multiple base changes were introduced by *Pfu*-turbo polymerase-based chain reaction using mutagenic oligonucleotides and the QuickChange site-directed mutagenesis kit (Stratagene, La Jolla, CA). The complete mutated sequences were confirmed by DNA sequencing and subcloned back into the *Cla1* and *Xba1* sites of pCMV5 vector containing the *EcoR1*/*Xba1* fragment of RyR1. Mutated full-length expression plasmids were prepared by ligation of three fragments (*Cla1*/*Xho1*, *Xho1*/*EcoR1*, *EcoR1*/*Xba1* containing the mutated sequence) and expression vector pCMV5 (*Cla1*/*Xba1*) as described (21). In this study, nucleotide and amino acid numbering are as described (4,22).

Expression of full-length wild-type and mutant RyRs in HEK 293 cells

RyR1 cDNAs were transiently expressed in HEK 293 cells transfected with FuGENE 6 (Roche Applied Science) according to the manufacturer's instructions. Cells were maintained at 37°C and 5% CO_2 in high glucose Dulbecco's modified Eagle's medium containing 10% fetal bovine serum and plated the day before transfection. For each 10-cm tissue culture dish, 3.5 μg of cDNA was used. Cells were harvested 48 h after transfection. Crude membrane fractions (21) and liposomes containing the purified 30S wild-type and mutant RyR1 ion channels (23) were prepared in the presence of protease inhibitors as described.

Ca^{2+} release measurements

Cellular Ca^{2+} release in response to caffeine was determined with the fluorescence Ca^{2+} indicator dye Fluo-4. HEK 293 cells transfected with cDNA encoding wild-type or mutant RyR1s were grown for 48 h on glass coverslips after transfection. Cells were washed three times with phosphate-buffered saline and loaded with 5 μM Fluo-4-AM for 1 h at 37°C in Krebs-Ringer-Henseleit (KRH) buffer (125 mM NaCl, 5 mM KCl, 1.2 mM KH_2PO_4, 6 mM glucose, 1.2 mM $MgCl_2$, 2 mM $CaCl_2$, and 25 mM HEPES, pH 7.4). After loading, the cells were rinsed with KRH buffer to remove nonhydrolyzed fluorophore and kept in KRH buffer for 30 min to complete de-esterification. For the Ca^{2+} release experiments, cells were transferred to a recording chamber with KRH buffer, and Fluo-4 fluorescence was recorded using a Photon Technology International (Lawrenceville, NJ) Deltascan system attached to an inverted microscope (TE 300; Nikon, Tokyo, Japan). Caffeine responsiveness of cells was recorded by rapid addition of freshly made caffeine solution to a final concentration of 10 mM. For analysis, individual cells were defined as region of interest, and average fluorescence was measured by using the program ImageMaster (Photon Technology International).

[^{3}H]Ryanodine binding

Unless otherwise indicated, crude membrane fractions prepared from HEK 293 cells were incubated with 2.5 nM [^{3}H]ryanodine in 20 mM imidazole, pH 7.0, 250 mM KCl, 150 mM sucrose, 1 mM glutathione (oxidized), protease inhibitors, and the indicated free Ca^{2+} concentrations. Nonspecific binding was determined using a 1000-fold excess of unlabeled ryanodine. After 20 h at 24°C, aliquots of the samples were diluted with 8.5 volumes of ice-cold water and placed on Whatman (Clifton, NJ) GF/B filters preincubated with 2% polyethyleneimine in water. Filters were washed with 3 $\times$ 5 ml ice-cold 0.1 M KCl, 1 mM KPipes, pH 7.0. Radioactivity remaining on the filters was determined by liquid scintillation counting to obtain bound [^{3}H]ryanodine.

Single-channel recordings

Single-channel measurements were performed using Mueller-Rudin type planar lipid bilayers containing a 5:3:2 mixture of bovine brain phosphatidylethanolamine, phosphatidylserine, and phosphatidylcholine (25 mg of total phospholipid/ml *n*-decane). Proteoliposomes containing the purified RyRs were added to the *cis* (satcoplasmic reticulum (SR) cytosolic side) chamber of a bilayer apparatus and fused in the presence of an osmotic gradient (250 mM *cis* KCl/20 mM *trans* KCl in 20 mM KHepes, pH 7.4, 2–20 μM Ca^{2+} with or without 1 mM ATP). After appearance of channel activity, *trans* (SR lumenal side) KCl concentration was increased to 250 mM to prevent further fusion of proteoliposomes. The *trans* side of the bilayer was defined as ground. The large cytosolic regulatory region of the channels faced the *cis* chamber in a majority (>98%) of the recordings (24). Electrical signals were filtered at 2 kHz (0.5 kHz for Ca^{2+} currents at 0 mV), digitized at 10 kHz, and analyzed as described (25).

To determine permeability ratios, single-channel activities were recorded in symmetrical 250 mM KCl solution with 10 mM Ca^{2+} on the *trans* side, and the reversal potential (E_{rev}) was measured. The permeability ratio of Ca^{2+} versus K^+ ions (P_{Ca}/P_K) was calculated using a modified form of the Goldman-Hodgkin-Katz equation

$$E_{rev} = -\frac{RT}{F} Ln\left\{ \left(\left(4\frac{P_{Ca}}{P_K}[Ca] + [K] \right)[K] \right)^{1/2} \times \left(4\frac{P_{Ca}}{P_K}[Ca] + [K] \right)^{-1} \right\},$$

where $[Ca]$ is the concentration of Ca^{2+} ions on *trans* side, and $[K]$ is the concentration of K^+ on the *cis* and *trans* sides.

The permeability ratio of ethylamine$^+$ versus K^+ (P_E/P_K) was determined by perfusing the *cis* chamber with 5 chamber volumes of 250 mM ethylamineCl in 10 mM TrisHepes, pH 7.4, 20 μM Ca^{2+}, and 1 mM ATP.

Biochemical assays and data analysis

Free Ca^{2+} concentrations were obtained by including in the solutions the appropriate amounts of Ca^{2+} and EGTA as determined by using the stability constants and computer program published by Schoenmakers et al. (26). Free Ca^{2+} concentrations of ≥ 1 μM were verified with the use of a Ca^{2+}-selective electrode.

Results are given as mean $\pm$ SE. Significance of differences in the data ($p < 0.05$) was determined using Student's *t*-test.

RESULTS

Fig. 1 shows the amino acid sequences of the pore-forming regions of the K^+ channel, KcsA, and the skeletal muscle ryanodine receptor, RyR1. Crystallographic analysis of the KcsA channel (Fig. 2) provides a basis for understanding the mechanism of rapid K^+ ion transport. The KcsA channel has four subunits with two transmembrane helices, a pore helix, the signature sequence TVGYG, and two linker regions per subunit. The interaction of the K^+ ions with the backbone carbonyl oxygen atoms of the signature sequence determines the selectivity of the KcsA channel (27).

The lumenal loop linking the two most C-terminal transmembrane spanning segments in RyR1 has a predicted pore helix and an amino acid motif (GGGIG) similar to the signature sequence (TVGYG) of KcsA (Fig. 1). A distinguishing feature is the many negatively charged amino acid residues in the two RyR1 regions linking the predicted pore helix and the two most C-terminal transmembrane spanning segments. In this study, we focused on the role of these residues in RyR1 ion permeation and selectivity. We removed by mutagenesis negative charges of amino acid residues conserved among the three mammalian RyRs (indicated in bold in Fig. 1). In the linker regions, we substituted glutamate with asparagine and aspartate with glutamine to determine the effect of both a change in side-chain length and charge. We also introduced one negative charge near the selectivity filter by substituting Ile 4901 with a glutamate residue. The expression levels and functional properties of the mutants were determined by immunoblot analysis, cellular fluorescence microscopy, and [^{3}H]ryanodine binding. Single-channel recordings determined the ion permeation properties of the mutants.

Functional properties of RyR1 pore mutants

Immunoblot analysis showed that all RyR1 mutants tested in this study were expressed in HEK 293 cells at a level comparable to wild-type (not shown). The fluorescence change of Fluo-4 was measured to detect Ca^{2+} release in response to 10 mM caffeine in wild-type (WT) and mutant RyR1s expressed in HEK 293 cells. Millimolar caffeine activates the purified RyR1 (28). Fig. 3 shows four representative Ca^{2+} release curves for vector (control), WT-RyR1, RyR1-D4899Q, and RyR1-E4900N transfected HEK 293 cells. Essentially identical time courses and peak amplitudes of Ca^{2+} release were observed for WT and mutant RyR1s, whereas vector transfected cells showed no caffeine response. Table 1 summarizes the caffeine response of 18 single-site mutants including four mutants (D4899N, D4903A, D4907A, D4917A) previously described (15). The mutants showed cellular Ca^{2+} release in response to 10 mM caffeine comparable to WT-RyR1, with the exception of D4873Q and D4917A, which displayed a background signal comparable to vector transfected cells.

The expression of functional RyR1 mutant proteins was also assessed by a [^{3}H]ryanodine binding assay. Ryanodine binds with high specificity to the RyRs and is widely used as a probe of channel activity because of its preferential binding to the open channel state (2,29). A majority of the mutants

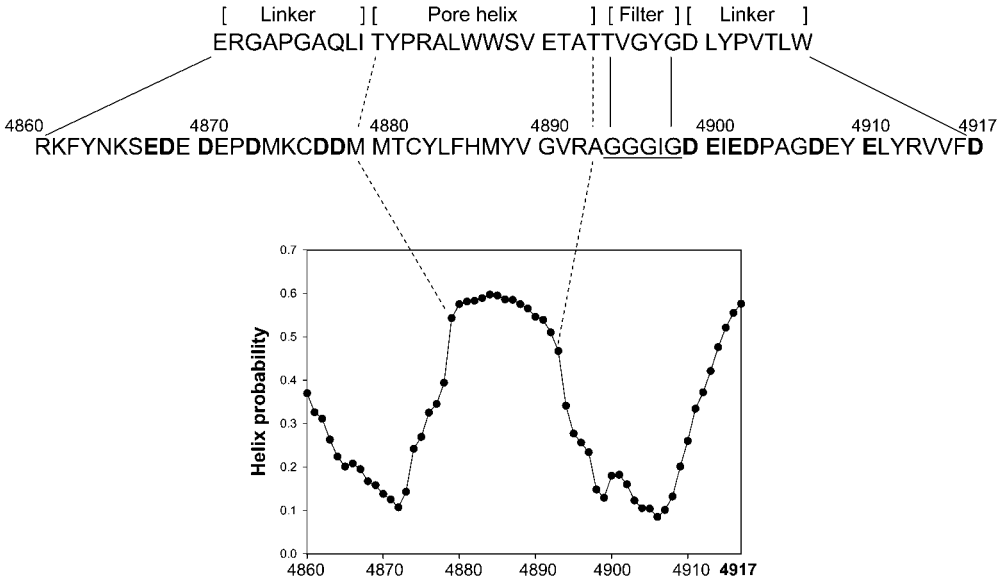

FIGURE 1 Pore-lining sequences of KcsA and RyR1 ion channels. Shown are the KcsA and putative RyR1 pore helix, selectivity filter, and linker regions. Bold indicates negatively charged amino acid residues identical in mammalian RyRs. Underlined amino acids indicate residues analogous to the selectivity filter of KcsA channel from *Streptomyces lividans* (8). Helical probability of putative RyR1 pore-lining region (*lower panel*) was calculated using a protein sequence analysis program (bmerc-www.bu.edu/psa/ (42)).

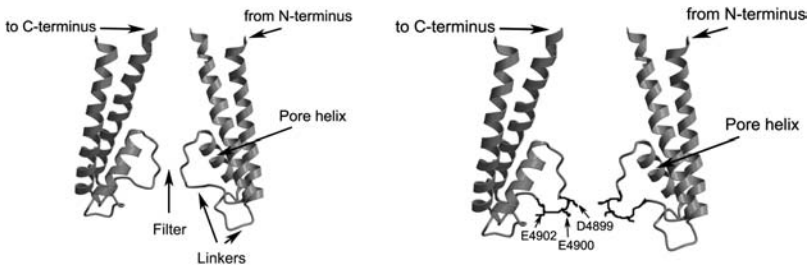

FIGURE 2 Hypothetical model for ion pore of RyR1. Secondary structure of potassium channel KcsA pore (*left*) and RyR1 pore (*right*). The RyR1 pore model, which was obtained by modifying by ''hand'' the published structure of KcsA (8), shows an extended C-terminal linker and the putative position of RyR1 amino acid residues D4899, E4900, and E4902. The two transmembrane spanning segments in RyR1 are analogous to S5 and S6 in 6TM K^+ channels (such as *Shaker* and KvAP) and M1 and M2 in 2TM K^+ channels (such as KcsA and Kir). Note only two of the four pore-forming segments are shown.

bound [^{3}H]ryanodine (Table 1) and showed Ca^{2+} dependence of [^{3}H]ryanodine binding close to the one shown for WT-RyR1 in Fig. 4. For two mutants immediately after the GGGIG motif (D4899E and D4899N), significantly lower binding values were observed at [Ca^{2+}] ≤ 1 μM, compared to WT-RyR1 (Fig. 4). Two mutants (D4873Q and D4917A) that failed to show a caffeine response also exhibited a loss of high-affinity [^{3}H]ryanodine binding. RyR1-I4901E exhibited a caffeine response but failed to bind [^{3}H]ryanodine, which indicated a loss of function during membrane isolation. The results of Figs. 3 and 4 suggest that a majority of the mutations investigated in this study did not introduce major global changes in protein conformation.

K^+ conductance of RyR1 mutant channels

To determine the ion permeation properties of the mutant RyR1 ion channels, single-channel measurements were performed using the planar lipid bilayer method. Proteoliposomes containing the purified 30S channel complexes were fused with planar lipid bilayers, and single channels were recorded in 250 mM KCl on both sides of the bilayer with K^+ as the current carrier. The *cis* (cytosolic) bilayer chamber contained micromolar activating Ca^{2+} (2–20 μM). In some recordings, 1 mM ATP was added to the *cis* chamber to increase single-channel activity. To ascertain retention of pharmacological regulation, cytosolic Ca^{2+} concentrations were reduced to 0.1 μM and increased to 100 μM. We found that all single-site mutants that both retained a caffeine response and bound [^{3}H]ryanodine exhibited a Ca^{2+} dependence similar to that of WT-RyR1 (not shown). RyR1-D4873Q, -I4901E, and -D4917A did not respond to a change in Ca^{2+} concentration and were not analyzed further.

The two mutations closest to the GGGIG sequence (D4899Q, D4899N) exhibited a greatly reduced K^+ conductance. In symmetrical 250 mM KCl, WT-RyR1 had

TABLE 1 Properties of RyR1 mutants

Name	Caffeine-induced Ca^{2+} release binding	[^{3}H]Ryanodine	K^+ conductance	I_{Ca}^{2+} at 0 mV	E_{rev}	P_{Ca}/P_K
			(pS)	(pA)	(mV)	
Vector	−	−				
WT-RyR1	+	+	801 ± 7(17)	−2.8 ± 0.1(7)	9.5 ± 0.2(6)	7.0
E4867N	+	+	790 ± 6(4)	−2.3 ± 0.1(3)*	9.2 ± 0.4(3)	6.7
D4868Q	+	+	814 ± 4(3)	−2.4 ± 0.2(3)	8.5 ± 0.3(3)*	6.0
D4870Q	+	+	813 ± 7(4)	−2.6 ± 0.1(4)	9.6 ± 0.2(4)	7.1
D4873Q	−	−				
D4877Q	+	+	810 ± 14(4)	−2.3 ± 0.1(3)*	9.5 ± 0.3(4)	7.0
D4878Q	+	+	800 ± 9(6)	−2.4 ± 0.1(4)*	10.2 ± 1.0(3)	7.8
D4899E	+	+	904 ± 3(16)*	−1.6 ± 0.3(4)*	10.0(2)	7.6
D4899N†‡	+	+		−0.4 ± 0.1(4)*	5.5 ± 1.2(4)*	3.4
D4899Q	+	+	164 ± 4(10)*	−0.4 ± 0.1(4)*	1.9 ± 0.1(4)*	1.0
E4900D	+	+	719 ± 8(7)*	−2.4(2)	10.0(2)	7.6
E4900N	+	+	505 ± 3(3)*	−2.0 ± 0.2(7)*	6.8 ± 0.4(5)*	4.5
E4900Q	+	+	450 ± 15(10)*	−1.4 ± 0.2(4)*	5.2 ± 0.9(4)*	3.2
I4901E	+	−				
E4902Q	+	+	782 ± 4(11)	−2.3 ± 0.1(5)*	9.0 ± 0.1(5)	6.5
D4903A†	+	+	796 ± 10(8)	−2.4 ± 0.2(4)	10.0(2)	7.6
D4907A†	+	+	790 ± 10(8)	−2.4 ± 0.2(4)	10.1(1)	7.6
E4910N	+	+	772 ± 8(5)	−2.1 ± 0.5(3)	9.0 ± 0.6(3)	6.5
D4917A†	−	−				

(+) Caffeine-induced Ca^{2+} release and [^{3}H]ryanodine binding activities comparable to WT-RyR1.
(−) No activity.
†Gao et al. (15), ‡145 ± 3 pS (10)* at +50 mV and 92 ± 3 pS (8)* at −50 mV, *$p < 0.05$.

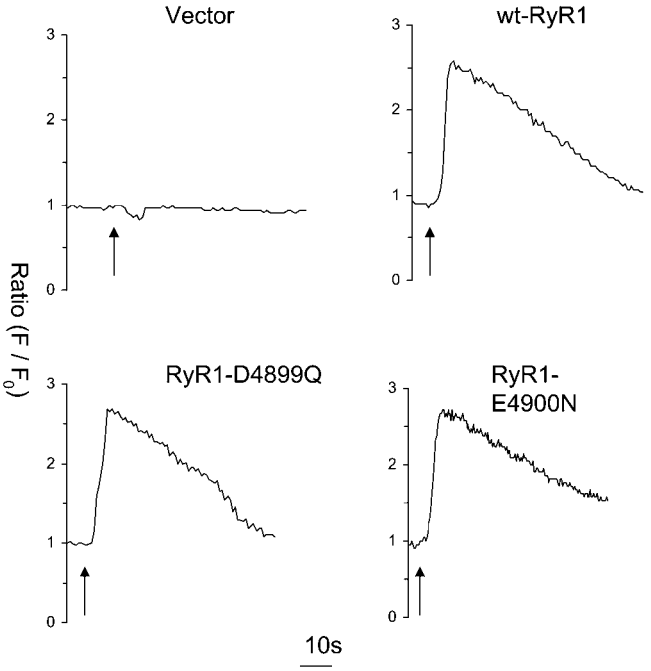

FIGURE 3 Caffeine-induced Ca^{2+} release in HEK 293 cells expressing WT-RyR1 and RyR1 mutants. HEK 293 cells were transfected with pCMV5 vector, WT-RyR1, RyR1-D4899Q, and -E4900N cDNA. The fluorescence intensity of Fluo-4 loaded cells was measured before and after addition of 10 mM caffeine. Arrows indicate the addition of caffeine. Representative traces are shown.

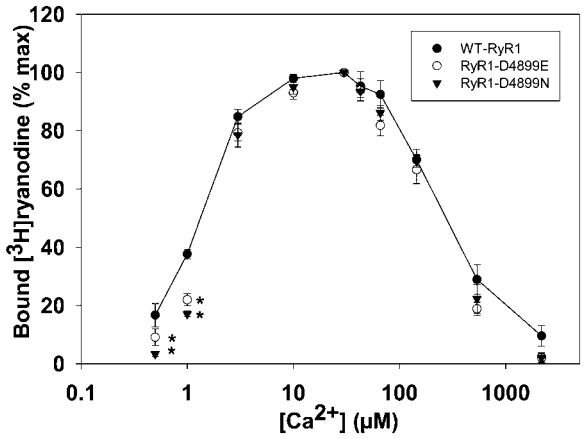

FIGURE 4 Ca^{2+} dependence of [^{3}H]ryanodine binding to WT-RyR1 and RyR1 mutants. Specific [^{3}H]ryanodine binding for cells transfected with WT-RyR1 (●), RyR1-D4899E (○), and RyR1-D4899N (▼) was determined as described under ''Experimental Procedures'' in 250 mM KCl, 150 mM sucrose, 20mM imidazole, pH 7.0, and 1 mM glutathione (oxidized) media containing 2.5 nM [^{3}H]ryanodine and the indicated concentrations of free Ca^{2+}. Data are mean ± SE of four experiments. *, $p < 0.05$ compared with wild-type.

a mean conductance of 801 ± 7 pS (Fig. 5), which was essentially identical to that of native skeletal muscle RyR1 (30). Removal of the negative charge in RyR1-D4899Q (Fig. 6) and -D4899N (15) significantly decreased K^+ conductance to 164 ± 4 and 145 ± 3 (at +50 mV), respectively (Table 1). The K^+ conductance of E4900Q and E4900N decreased to a lesser extent than those in the corresponding D4899 mutants (Table 1). By comparison, mutants farther from the GGGIG sequence (with either an aspartate to glutamine or glutamate to asparagine substitution) showed a K^+ conductance close to wild-type (Table 1). The K^+ currents measured in symmetrical 250 mM KCl at potentials ranging from −50 mV to +50 mV showed a linear voltage dependence similar to that of wild type (Fig. 5 *C*), with the exception of D4899N, which exhibited a nonlinear voltage dependence (15). We conclude that the two negatively charged amino acid residues D4899 and E4900 support the high rates of RyR ion flux.

Given the importance of D4899 and E4900 in determining the K^+ conductance of RyR1, we further analyzed the effects of a change in the length of their side chains and neutralization of their charges. Chain length was altered by substitution of D4899 with glutamate (Fig. 7) and E4900 with aspartate (not shown). In both positions, the longer side chain supported an ~10% higher K^+ conductance. Substitution of D4899 with a glutamate residue increased K^+ conductance from 801 ± 7 pS to 904 ± 3 pS, whereas replacement of E4900 with an aspartate residue decreased K^+ conductance to 719 ± 8 pS (Table 1). Measurement of conductance and concentration relationships showed that the K^+ conductance of wild-type, D4899Q, and E4900N reached a plateau with the ion concentration increase (Fig. 8). The data could be reasonably fit assuming a single binding site. The apparent K_D value of 98 mM for D4899Q was significantly higher than the K_D values of 23 mM and 28 mM for E4900N and WT-RyR1, respectively. The results indicate that the negative charge of D4899 strongly interacts with K^+. A change in apparent binding affinity, however, cannot fully explain that the mutant channels maintain a much reduced K^+ conductance at elevated K^+ concentrations.

RyR1-D4899Q is a cation-selective ion channel

To determine whether the mutations created an anion-conducting channel, we measured the reversal potentials for RyR1-D4899Q in asymmetric KCl solutions. Fig. 9 shows the current-voltage relationships of recordings with 250 mM KCl on both sides of the bilayer and in two asymmetric solutions containing 250 mM *cis* KCl and 20 mM or 50 mM *trans* KCl. In the asymmetric KCl solutions, the measured reversal potentials matched the calculated reversal potential within the error of the measurements, as determined by the Nernst equation. The result suggests that like WT-RyR1, RyR1-D4899Q forms a cation-selective ion channel.

Cation selectivity of RyR1 mutants

RyRs have a higher ion conductance for monovalent than divalent cations, yet they permeate the physiologically more

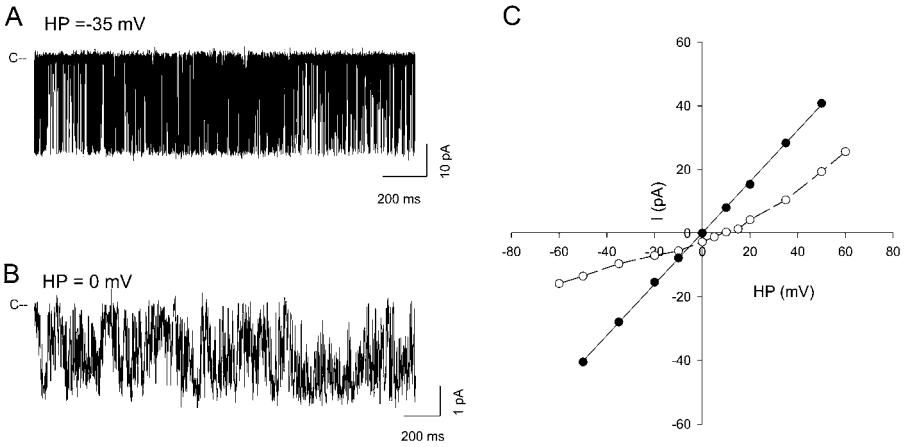

FIGURE 5 Single-channel recordings of WT-RyR1. (*A*) Single-channel currents were recorded at −35 mV in symmetrical 250 mM KCl with 2 μM Ca^{2+} and are shown as downward inflections from the closed state (*c*–). (*B*) Single-channel currents recorded at 0 mV in symmetrical 250 mM KCl with 10 mM *trans* Ca^{2+} and 20 μM *cis* Ca^{2+} plus 1 mM ATP. (*C*) Current-voltage relationship in 250 mM symmetrical KCl (●, $n = 17$) and with the subsequent addition of 10 mM *trans* Ca^{2+} (○, $n = 7$).

relevant Ca^{2+} with a higher selectivity than K^+ (12–14). To determine the Ca^{2+} selectivity of the RyR1 mutants, current-voltage curves were recorded in 250 mM symmetrical KCl with and without 10 mM Ca^{2+} in the *trans* (SR lumenal) bilayer chamber. The single-channel currents and current-voltage relationships of wild-type (Fig. 5), RyR1-D4899Q (Fig. 6), and RyR1-D4899E (Fig. 7) are shown in the presence (*open circles*) and absence (*filled circles*) of 10 mM *trans* Ca^{2+}. The potassium currents were linear in the absence of 10 mM *trans* Ca^{2+}. Addition of 10 mM Ca^{2+} to the *trans* chamber reduced single-channel gating (Figs. 5 *B*, 6 *B*, and 7 *B*) and channel currents at elevated positive and negative potentials. At 0 mV, a current of −2.8 pA for WT-RyR1 and reduced currents of −1.6 and −0.4 pA for RyR1-D4899E and RyR1-D4899Q were measured (Table 1). Addition of 10 mM *trans* Ca^{2+} greatly reduced D4899Q (Fig. 6 *B*), D4899E (Fig. 7 *B*), and RyR1-E4900D (not shown) single-channel activities. Channel openings were only observed over the whole voltage range in ~1 of 5 RyR1-D4899E and RyR1-E4900D recordings, limiting the number of E_{rev} determinations. Single-channel currents of some of the remaining mutants were also reduced at 0 mV, with the greatest reduction being observed, in addition to D4899E and D4899Q, for D4899N followed by E4900Q and E4900N (Table 1). The reversal potentials (E_{rev}) for WT-RyR1 and RyR1-D4899Q were shifted to +9.5 and +1.9 mV with the addition of Ca^{2+}, respectively, from which, applying constant field theory, permeability ratios of Ca^{2+} over K^+ (P_{Ca}/P_K) of 7.0 and 1.0 were calculated. Compared to wild-type, lower P_{Ca}/P_K ratios were also calculated for RyR1-D4899N, E4900N, and E4900Q. By comparison, replacement of aspartate and glutamate residues with glutamine and asparagine residues in the linker regions bridging the two most C-terminal membrane spanning and pore helices showed only small changes in P_{Ca}/P_K values compared to wild-type.

The permeability properties of the mutant receptors were also examined, using an organic cation (ethanolamine) with a size approaching that of the diameter of RyR2 selectivity filter (9). We determined whether our mutations affected the permeability of ethylamine$^+$ relative to that of K^+ (P_E/P_K) for WT-RyR1, RyR1-D4899E, -D4899N, -D4899Q, -E4900N, and -E4900Q by replacing K^+ with ethylamine$^+$ in the *cis* bilayer chamber. Representative recordings of the current-voltage relationships of WT-RyR1 and RyR1-D4899Q are shown in Fig. 10. WT-RyR1 and all mutants exhibited a greatly reduced conductance at +50 mV compared to −50 mV (Table 2), suggesting a reduced conductance for

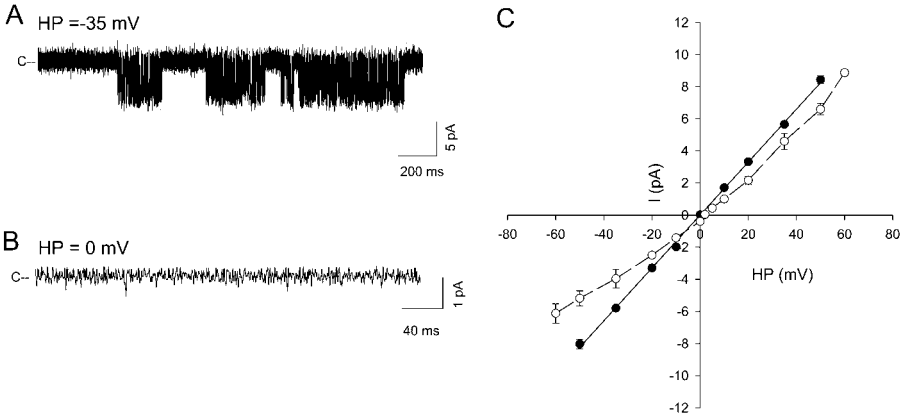

FIGURE 6 Single-channel recordings of RyR1-D4899Q. (*A*) Single-channel currents were recorded at −35 mV in symmetrical 250 mM KCl with 2 μM Ca^{2+} and are shown as downward inflections from the closed state (*c*–). Note the long channel closings that are absent from WT-RyR1 (Fig. 5). (*B*) Single-channel currents recorded at 0 mV in symmetrical 250 mM KCl with 10 mM *trans* Ca^{2+} and 20 μM *cis* Ca^{2+} plus 1 mM ATP. (*C*) Current-voltage relationship in 250 mM symmetrical KCl (●, $n = 10$) and with the subsequent addition of 10 mM *trans* Ca^{2+} (○, $n = 4$).

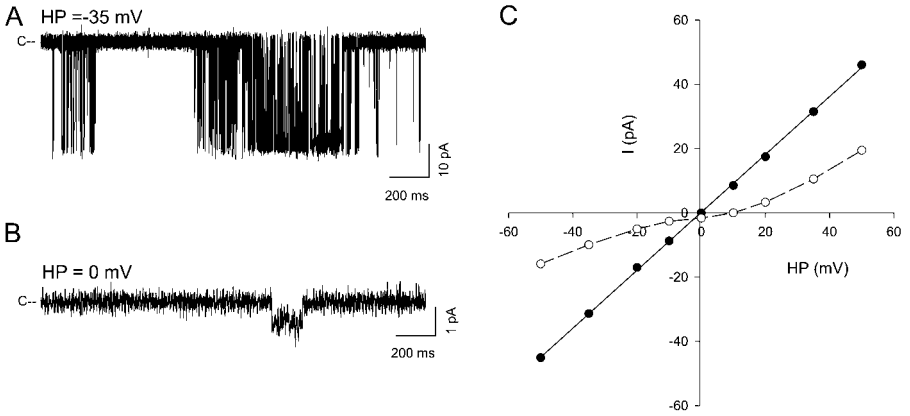

FIGURE 7 Single-channel recordings of RyR1-D4899E. (*A*) Single-channel currents were recorded at −35 mV in symmetrical 250 mM KCl with 2 μM Ca^{2+} and are shown as downward inflections from the closed state (*c*–). Note the long channel closings that are absent from WT-RyR1 (Fig. 5). (*B*) Single-channel currents recorded at 0 mV in symmetrical 250 mM KCl with 10 mM *trans* Ca^{2+} and 20 μM *cis* Ca^{2+} plus 1 mM ATP (*C*) Current-voltage relationship in 250 mM symmetrical KCl (●, $n = 16$) and with the subsequent addition of 10 mM *trans* Ca^{2+} (○, $n = 2$).

ethylamine$^+$ compared to K^+. The reversal potential (E_{rev}) and P_E/P_K ratio of the mutants did not significantly differ from that of WT-RyR1 (Table 2), with the exception of D4899Q. The E_{rev} was shifted to the right for D4899Q, resulting in a significantly lower P_E/P_K ratio. The changes in the permeability ratio of D4899Q are indicative of a decrease in the radius of the pore although other factors cannot be ruled out (31). Notably, the same permeability ratio was obtained when the charge was retained (WT and D4899E) but was different when the charge was taken away (D4899Q and D4899N). This indicates the predominance of charge in determining the ion permeability properties of the RyRs.

DISCUSSION

In this study, the known structure of the bacterial K^+ channel KcsA was used as a guide to neutralize by mutagenesis the negative charge of 10 conserved aspartate and glutamate residues in the predicted pore region of the RyRs. Although the pore region of the RyR ion channels has a predicted architecture similar to that of K^+ channels (15,16,32–34), there exist significant functional and sequence differences. First, the physiological role of K^+ channels is to selectively conduct K^+ ions. In comparison, SR Ca^{2+} release is not dependent on a highly selective Ca^{2+} channel because ions on both sides of the sarcoplasmic reticulum are at equilibrium in resting cells with the exception of Ca^{2+} (35). Second, RyR has a high ion conductance for both monovalent cations (~800 pS with 250 mM K^+ as conducting ion) and divalent cations (~150 pS with 50 mM Ca^{2+}). Third, the RyR pore has a minimum radius of 3.5 Å as estimated from the relative permeability of organic cations (9), as compared to a radius of ~1.5 Å for the KcsA channel (27). Fourth, the RyRs have a conserved DE motif in close proximity to the GGGIG motif. In contrast, the aspartate residue in the K^+ channels immediately after the TVGYG motif is not fully conserved, and the residue after the aspartate residue is a neutral or positively charged amino acid (8). These differences suggest

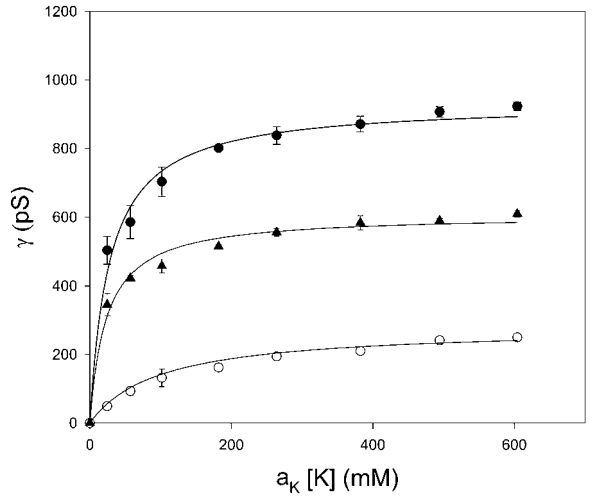

FIGURE 8 Conductance −K^+ activity relationships of WT-RyR1 and RyR1 mutants. Shown are the effects of increasing K^+ activity on single-channel conductances of WT-RyR1 (●), RyR1-E4900N (▲), and RyR1-D4899Q (○). Data are the mean of at least three experiments ± SE. The K_D values and maximum conductances (γ_{max}) obtained by nonlinear regression analysis are 28 mM and 934 pS for WT-RyR1, 23 mM and 607 pS for E4900N, and 98 mM and 280 pS for D4899Q.

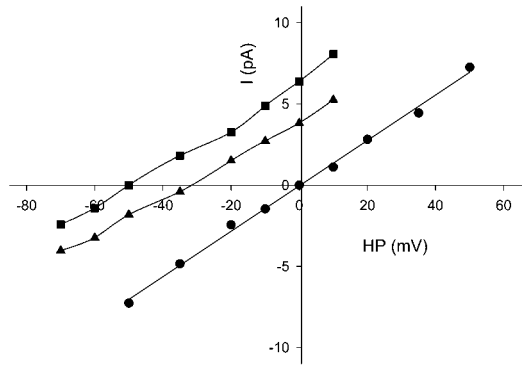

FIGURE 9 Current-voltage relationships of RyR1-D4899Q. Single channels were recorded in 250 mM KCl *cis*/250 mM KCl *trans* (●), 250 mM KCl *cis*/50 mM KCl *trans* (▲), 250 mM KCl *cis*/20 mM KCl *trans* (■). The measured and calculated reversal potentials in the two asymmetric KCl media were 32 and 34 mV (▲) and 50 and 48 mV (■), respectively. One of two recordings is shown.

TABLE 2 Wild-type and mutant RyR1 ion conductances in 250 mM *trans* K^+ and 250 mM *cis* ethanolamine$^+$ media

WT-RyR1 and mutants	Conductance at −50 mV	Conductance at +50 mV	E_{rev}	P_E/P_K
	(pS)	(pS)	(mV)	
WT-RyR1	567 ± 12(4)	91 ± 9(4)	18.3 ± 0.7(4)	0.48
D4899E	673(2)*	101(2)	17.9 ± 0.3(4)	0.49
D4899N	73(2)*	39(1)	22.2 ± 1.9(3)	0.41
D4899Q	94(2)*	18 ± 2(4)*	30.0 ± 1.7(5)*†	0.30*†
E4900N	355(2)*	64 ± 6(3)	16.8 ± 0.6(7)	0.51
E4900Q	313 ± 8(5)*	58 ± 6(5)*	17.2 ± 1.4(5)	0.51

*$p < 0.05$ compared with WT-RyR1.
†$p < 0.05$ D4899Q compared with D4899N.

that the two ion channel families may use different principles in controlling the rates of ion translocation.

This study shows that the DE motif plays a critical role in RyR1 ion permeation and selectivity. We found that charge neutralization of two RyR1 residues (D4899, E4900) immediately after the GGGIG motif (TYGYG in KcsA) reduced the ion conductance and selectivity for Ca^{2+} compared to K^+. Charge neutralization of acidic amino acids farther from the GGGIG motif showed only small changes in ion conductance and selectivity. The results show that the negative charges on the side chains of D4899 (and to a lesser extent, E4900) determine the majority of RyR ion conductance and selectivity. The DDDD motif in the selectivity filter of the tetrameric RyR1 is not without precedence. A DDDD/EEEE motif has a critical role in ion selectivity and permeation of L-type Ca^{2+} channel (36) and glutamate (37) and vanilloid (38) receptor ion channels.

We have shown that the current-voltage relationships of RyR (native and mutants D4899N and E4900Q) are well reproduced by an ion permeation model that exclusively models the negatively charged carboxyl oxygens of D4899 and E4900 (20). The Poisson-Nernst-Planck/Density Functional Theory model (39) describes the electrodiffusion of hard-sphere ions down their chemical potential gradients. The occupancy of the channel is a result of the ions' attraction to the channel by the negative charges of the channel protein (specifically D4899 and E4900) and the competition for space inside the very small selectivity filter. The model differs from others in that it uses the mutant data to construct the RyR selectivity filter instead of data fitting critical channel parameters (40,41).

We present a hypothetical model for the ion pore of RyR1 in Fig. 2. The model proposes that the RyR1 pore (*right*) has architecture similar to that of KcsA (*left*), with three important differences. The RyR model has an extended C-terminal linker, the pore is wider, and the eight negative charges of D4899 and E4900 (only two are shown for each) are placed in and near the selectivity filter. In a recent article, molecular dynamic simulations identified several kinetically important residues that slowed the velocity of K^+ and Ca^{2+} movement through the RyR2 pore (34). At variance with the experimental results of this study, RyR2-D4830 (equivalent to RyR1-D4899) was not identified as a major kinetic barrier that reduced the rates of ion translocation.

Besides its role in ion permeation and selectivity, this study also confirms results of previous studies that indicated mutations at the 4899 position affect RyR channel function and stability. In two studies, RyR1-D4899A and -D4899R (15) and the equivalent RyR2-D4830A (17) showed loss of high-affinity [^{3}H]ryanodine binding but maintained caffeine-induced Ca^{2+} release in HEK cells, indicating a loss of function during membrane isolation. In another study,

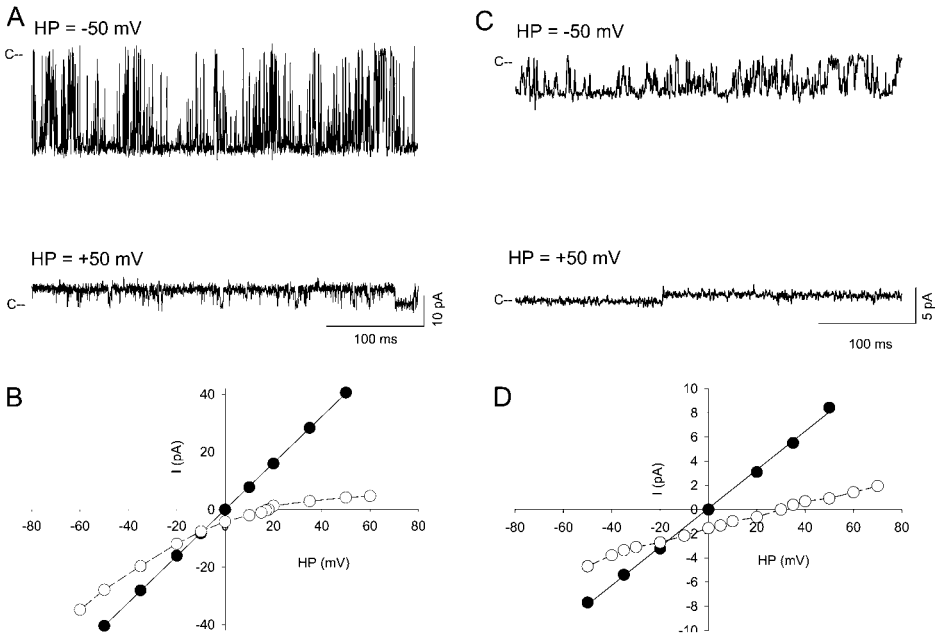

FIGURE 10 WT-RyR1 and RyR1-D4899Q conductances in 250 mM *trans* KCl and 250 mM *cis* ethanolamineCl media. WT-RyR1 (*A*) and RyR1-D4899Q (*C*) single-channel currents were recorded in 250 mM *cis* ethylamineCl with 20 μM Ca^{2+} plus 1 mM ATP *cis* and 250 mM KCl *trans* at −50mV (*upper trace*) and +50 mV (*lower trace*). WT-RyR1 (*B*) and RyR1-D4899Q (*D*) current-voltage relationships in 250 mM symmetrical KCl (●) and after perfusion of the *cis* chamber with five chamber volumes of 250 mM ethylamineCl (○).

RyR2-D4830A exhibited increased rates of [^{3}H]ryanodine binding/dissociation and a reduced single-channel conductance of 160 pS (16).

In this study we found that D4899E has a reduced Ca^{2+} dependence of [^{3}H]ryanodine binding at low [Ca^{2+}], indicating that even a fairly benign substitution affects some functional aspects of RyR1. D4899N had a similar reduction in Ca^{2+} dependence of [^{3}H]ryanodine binding at low [Ca^{2+}], and both D4899E and D4899Q had a significant decrease in open probability in the presence of *trans* Ca^{2+}. Furthermore, RyR1-D4899N differed from that of the similar D4899Q mutation by having a nonlinear current-voltage relationship. D4899E also had a slightly higher conductance than WT. Taken together, these results indicate that D4899 is also involved in the Ca^{2+} dependence of both [^{3}H]ryanodine binding and gating and that substitutions at this site may cause some conformational changes.

This work was supported by National Institutes of Health grants AR18687 and HL 73051 (to G.M.) and GM 067241 (to D.G.).

REFERENCES

1. Fill, M., and J. A. Copello. 2002. Ryanodine receptor calcium release channels. *Physiol. Rev.* 82:893–922.
2. Franzini-Armstrong, C., and F. Protasi. 1997. Ryanodine receptors of striated muscles: a complex channel capable of multiple interactions. *Physiol. Rev.* 77:699–729.
3. Meissner, G. 2002. Regulation of mammalian ryanodine receptors. *Front. Biosci.* 7:d2072–d2080.
4. Takeshima, H., S. Nishimura, T. Matsumoto, H. Ishida, K. Kangawa, N. Minamino, H. Matsuo, M. Ueda, M. Hanaoka, T. Hirose, and S. Numa. 1989. Primary structure and expression from complementary DNA of skeletal muscle ryanodine receptor. *Nature.* 339:439–445.
5. Zorzato, F., J. Fujii, K. Otsu, M. Phillips, N. M. Green, F. A. Lai, G. Meissner, and D. H. MacLennan. 1990. Molecular cloning of cDNA encoding human and rabbit forms of the Ca^{2+} release channel (ryanodine receptor) of skeletal muscle sarcoplasmic reticulum. *J. Biol. Chem.* 265:2244–2256.
6. Du, G. G., B. Sandhu, V. K. Khanna, X. H. Guo, and D. H. MacLennan. 2002. Topology of the Ca^{2+} release channel of skeletal muscle sarcoplasmic reticulum (RyR1). *Proc. Natl. Acad. Sci. USA.* 99:16725–16730.
7. Wagenknecht, T., and M. Samso. 2002. Three-dimensional reconstruction of ryanodine receptors. *Front. Biosci.* 7:d1464–d1474.
8. Doyle, D. A., J. Morais Cabral, R. A. Pfuetzner, A. Kuo, J. M. Gulbis, S. L. Cohen, B. T. Chait, and R. MacKinnon. 1998. The structure of the potassium channel: molecular basis of K^+ conduction and selectivity. *Science.* 280:69–77.
9. Tinker, A., and A. J. Williams. 1993. Probing the structure of the conduction pathway of the sheep cardiac sarcoplasmic reticulum calcium-release channel with permeant and impermeant organic cations. *J. Gen. Physiol.* 102:1107–1129.
10. Tinker, A., and A. J. Williams. 1995. Measuring the length of the pore of the sheep cardiac sarcoplasmic reticulum calcium release channel using related trimethylammonium ions as molecular calipers. *Biophys. J.* 68:111–120.
11. Tu, Q., P. Velez, M. Brodwick, and M. Fill. 1994. Streaming potentials reveal a short ryanodine-sensitive selectivity filter in cardiac Ca^{2+} release channel. *Biophys. J.* 67:2280–2285.
12. Liu, Q. Y., F. A. Lai, E. Rousseau, R. V. Jones, and G. Meissner. 1989. Multiple conductance states of the purified calcium release channel complex from skeletal sarcoplasmic reticulum. *Biophys. J.* 55:415–424.
13. Smith, J. S., T. Imagawa, J. Ma, M. Fill, K. P. Campbell, and R. Coronado. 1988. Purified ryanodine receptor from rabbit skeletal muscle is the calcium-release channel of sarcoplasmic reticulum. *J. Gen. Physiol.* 92:1–26.
14. Tinker, A., and A. J. Williams. 1992. Divalent cation conduction in the ryanodine receptor channel of sheep cardiac muscle sarcoplasmic reticulum. *J. Gen. Physiol.* 100:479–493.
15. Gao, L., D. Balshaw, L. Xu, A. Tripathy, C. Xin, and G. Meissner. 2000. Evidence for a role of the lumenal M3–M4 loop in skeletal muscle Ca^{2+} release channel (ryanodine receptor) activity and conductance. *Biophys. J.* 79:828–840.
16. Chen, S. R., P. Li, M. Zhao, X. Li, and L. Zhang. 2002. Role of the proposed pore-forming segment of the Ca^{2+} release channel (ryanodine receptor) in ryanodine interaction. *Biophys. J.* 82:2436–2447.
17. Du, G. G., X. Guo, V. K. Khanna, and D. H. MacLennan. 2001. Functional characterization of mutants in the predicted pore region of the rabbit cardiac muscle Ca^{2+} release channel (ryanodine receptor isoform 2). *J. Biol. Chem.* 276:31760–31771.
18. Zhao, M., P. Li, X. Li, L. Zhang, R. J. Winkfein, and S. R. Chen. 1999. Molecular identification of the ryanodine receptor pore-forming segment. *J. Biol. Chem.* 274:25971–25974.
19. Dirksen, R. T., and G. Avila. 2002. Altered ryanodine receptor function in central core disease: leaky or uncoupled Ca^{2+} release channels? *Trends Cardiovasc. Med.* 12:189–197.
20. Gillespie, D., G. Meissner, and L. Xu. 2005. Ion permeation model of ryanodine receptor. *Biophys. J.* 88:488a.(Abstr.)
21. Gao, L., A. Tripathy, X. Lu, and G. Meissner. 1997. Evidence for a role of C-terminal amino acid residues in skeletal muscle Ca^{2+} release channel (ryanodine receptor) function. *FEBS Lett.* 412:223–226.
22. Nakai, J., T. Imagawa, Y. Hakamata, M. Shigekawa, H. Takeshima, and S. Numa. 1990. Primary structure and functional expression from cDNA of the cardiac ryanodine receptor/calcium release channel. *FEBS Lett.* 271:169–177.
23. Lee, H. B., L. Xu, and G. Meissner. 1994. Reconstitution of the skeletal muscle ryanodine receptor-Ca^{2+} release channel protein complex into proteoliposomes. *J. Biol. Chem.* 269:13305–13312.
24. Xu, L., and G. Meissner. 1998. Regulation of cardiac muscle Ca^{2+} release channel by sarcoplasmic reticulum lumenal Ca^{2+}. *Biophys. J.* 75:2302–2312.
25. Stange, M., L. Xu, D. Balshaw, N. Yamaguchi, and G. Meissner. 2003. Characterization of recombinant skeletal muscle (Ser-2843) and cardiac muscle (Ser-2809) ryanodine receptor phosphorylation mutants. *J. Biol. Chem.* 278:51693–51702.
26. Schoenmakers, T. J., G. J. Visser, G. Flick, and A. P. R. Theuvenet. 1992. CHELATOR: an improved method for computing metal ion concentrations in physiological solutions. *Biotechniques.* 12:870–879.
27. MacKinnon, R. 2003. Potassium channels. *FEBS Lett.* 555:62–65.
28. Rousseau, E., J. Ladine, Q. Y. Liu, and G. Meissner. 1988. Activation of the Ca^{2+} release channel of skeletal muscle sarcoplasmic reticulum by caffeine and related compounds. *Arch. Biochem. Biophys.* 267:75–86.
29. Sutko, J. L., J. A. Airey, W. Welch, and L. Ruest. 1997. The pharmacology of ryanodine and related compounds. *Pharmacol. Rev.* 49:53–98.
30. Xu, L., R. Jones, and G. Meissner. 1993. Effects of local anesthetics on single channel behavior of skeletal muscle calcium release channel. *J. Gen. Physiol.* 101:207–233.
31. Gillespie, D., and R. S. Eisenberg. 2002. Physical descriptions of experimental selectivity measurements in ion channels. *Eur. Biophys. J.* 31:454–466.
32. Balshaw, D., L. Gao, and G. Meissner. 1999. Lumenal loop of the ryanodine receptor: a pore-forming segment? *Proc. Natl. Acad. Sci. USA.* 96:3345–3347.

33. Lee, J. M., S. H. Rho, D. W. Shin, C. Cho, W. J. Park, S. H. Eom, J. Ma, and D. Han Kim. 2004. Negatively charged amino acids within the intraluminal loop of ryanodine receptor are involved in the interaction with triadin. *J. Biol. Chem.* 279:6994–7000.

34. Welch, W., S. Rheault, D. J. West, and A. J. Williams. 2004. A model of the putative pore region of the cardiac ryanodine receptor channel. *Biophys. J.* 87:2335–2351.

35. Meissner, G. 1983. Monovalent ion and calcium ion fluxes in sarcoplasmic reticulum. *Mol. Cell. Biochem.* 55:65–82.

36. Heinemann, S. H., H. Terlau, W. Stuhmer, K. Imoto, and S. Numa. 1992. Calcium channel characteristics conferred on the sodium channel by single mutations. *Nature*. 356:441–443.

37. Panchenko, V. A., C. R. Glasser, and M. L. Mayer. 2001. Structural similarities between glutamate receptor channels and K^+ channels examined by scanning mutagenesis. *J. Gen. Physiol.* 117:345–359.

38. García-Martínez, C., C. Morenilla-Palao, R. Planells-Cases, J. M. Merino, and A. Ferrer-Montiel. 2000. Identification of an aspartic residue in the P-loop of the vanilloid receptor that modulates pore properties. *J. Biol. Chem.* 275:32552–32558.

39. Gillespie, D., W. Nonner, and R. S. Eisenberg. 2002. Coupling Poisson-Nernst-Plank and density functional theory to calculate ion flux. *J. Phys. Condens. Matter*. 14:12129–12145.

40. Tinker, A., A. R. G. Lindsay, and A. Williams. 1992. A model for ionic conduction in the ryanodine receptor channel of sheep cardiac muscle sarcoplasmic reticulum. *J. Gen. Physiol.* 100:495–517.

41. Chen, D. P., L. Xu, B. Eisenberg, and G. Meissner. 2003. Calcium ion permeation through the calcium release channel (ryanodine receptor) of cardiac muscle. *J. Phys. Chem. B*. 107:9139–9145.

42. Stultz, C. M., R. Nambudripad, R. H. Lathrop, and J. V. White. 1997. Predicting protein structure with probabilistic models. *In* Protein Structural Biology in Bio-Medical Research, Vol. 22B. N. Allewell and C. Woodward, editors. Advances in Molecular and Cell Biology, E. E. Bittar, series editor. JAI Press, Greenwich, CT. 447–506.